Available online at www.sciencedirect.com

ScienceDirect

Geochimica et Cosmochimica Acta 180 (2016) 109–125

Geochimica et Cosmochimica Acta

www.elsevier.com/locate/gca

Beryllium-7 and lead-210 chronometry of modern soil processes: The Linked Radionuclide aCcumulation model, LRC

Joshua D. Landis [a,*], Carl E. Renshaw [a], James M. Kaste [b]

[a] Department of Earth Science, Dartmouth College, 6105 Fairchild Hall, Hanover, NH 03755, USA
[b] Geology Department, The College of William and Mary, McGlothlin-Street Hall 217, Williamsburg, VA 23187, USA

Received 14 July 2015; accepted in revised form 11 February 2016; available online 16 February 2016

Abstract

Soil systems are known to be repositories for atmospheric carbon and metal contaminants, but the complex processes that regulate the introduction, migration and fate of atmospheric elements in soils are poorly understood. This gap in knowledge is attributable, in part, to the lack of an established chronometer that is required for quantifying rates of relevant processes. Here we develop and test a framework for adapting atmospheric lead-210 chronometry (^{210}Pb; half-life 22 years) to soil systems. We propose a new empirical model, the Linked Radionuclide aCcumulation model (LRC, aka "lark"), that incorporates measurements of beryllium-7 (^{7}Be; half-life 54 days) to account for ^{210}Pb penetration of the soil surface during initial deposition, a process which is endemic to soils but omitted from conventional ^{210}Pb models (e.g., the Constant Rate of Supply, CRS model) and their application to sedimentary systems. We validate the LRC model using the 1963–1964 peak in bomb-fallout americium-241 (^{241}Am; half-life of 432 years) as an independent, corroborating time marker. In three different soils we locate a sharp ^{241}Am weapons horizon at disparate depths ranging from 2.5 to 6 cm, but with concordant ages averaging 1967 ± 4 via the LRC model. Similarly, at one site contaminated with mercury (Hg_T) we find that the LRC model is consistent with the recorded history of Hg emission. The close agreement of Pb, Am and Hg behavior demonstrated here suggests that organo-metallic colloid formation and migration incorporates many trace metals in universal soil processes and that these processes may be described quantitatively using atmospheric ^{210}Pb chronometry. The ^{210}Pb models evaluated here show that migration rates of soil colloids on the order of 1 mm yr^{-1} are typical, but also that these rates vary systematically with depth and are attributable to horizon-specific processes of leaf-litter decay, eluviation and illuviation. We thus interpret ^{210}Pb models to quantify (i) exposure of the soil system to atmospheric aerosol deposition in the context of (ii) organic carbon assimilation, colloid production, and advection through the soil profile. The behavior of some other elements, such as Cs, diverges from the conservative colloid behavior exemplified by Pb and Am, and in these cases the value of empirical ^{210}Pb chronometry models like LRC and CRS is as a comparator rather than as an absolute chronometer. We conclude that ^{210}Pb chronometry is valuable for tracing colloidally-mediated transport of Pb and similarly-refractory metals, as well as the mobile pool of carbon in soils.

1. INTRODUCTION

Soils function as repositories for atmospheric carbon (Dixon et al., 1994; Schimel, 1995; Schmidt et al., 2011), metal contaminants including Pb (Steinnes and Friedland, 2005; Ma et al., 2014) and Hg (Mason et al., 1994; Obrist et al., 2011), and nuclear bomb and reactor fallout

* Corresponding author.
E-mail address: joshua.d.landis@dartmouth.edu (J.D. Landis).

http://dx.doi.org/10.1016/j.gca.2016.02.013
0016-7037/

(UNSCEAR, 2000; Yasunari et al., 2011). While the fate of carbon and persistent contaminants in soils is a growing concern due to the cumulative effect of ongoing anthropogenic emissions (Nriagu and Pacyna, 1988; Nriagu, 1988; Prestbo and Gay, 2009; Schmidt et al., 2011), our understanding of the processes that govern the introduction, transport and fate of atmospheric elements in soils is poor. This gap in our understanding of contaminant behavior is attributable, in part, to the absence of an established, universal chronometer for tracing relevant soil processes. In sedimentary records such as ice cores (Wang et al., 2014), lacustrine and marine sediment deposits (Conroy et al., 2008; Beal et al., 2014), and peat accumulations (Chambers et al., 2007; Mackay et al., 2014), naturally-occurring fallout lead-210 (^{210}Pb) has proven to be a valuable chronometer and a critical tool for revealing environmental change. This is due to the global distribution of atmospheric ^{210}Pb (Robbins, 1978; Preiss et al., 1996) and the congruence of its half-life (22.3 years) with the timescale of high-impact anthropogenic activities and industrial emissions. Atmospheric ^{210}Pb ('excess' or $^{210}Pb_{xs}$) accumulates in sedimentary glacial, lacustrine and peat layers during their surficial exposure, and upon sequential burial of each layer ^{210}Pb provides a clock as a consequence of its radioactive decay (Krishnaswamy et al., 1971).

But the applicability of ^{210}Pb chronometry to soils is uncertain because soil processes are more complicated than the sequential burial of layers. Conventional ^{210}Pb models thus lack a conceptual basis for their application to soils. Unlike sedimentary systems where ^{210}Pb is interpreted as a passive marker of sediment accretion, in soils we propose that the behavior of ^{210}Pb follows organo-metallic colloid migration. This behavior is consistent with observations that, through soil processes including atmospheric deposition (Murozumi et al., 1969), percolation, eluviation, sequestration, circulation (Greeman et al., 1999; Kaste et al., 2011a), and organic litter accumulation and decay, Pb is strongly retained by organic matter (Erel et al., 1990; Miller and Friedland, 1994; Wang and Benoit, 1997; Klaminder et al., 2006), forms stable organo-metallic complexes (Kerndorff and Schnitzer, 1980; Kaste et al., 2005) and is eluviated in an organic, particulate phase (Miller and Friedland, 1994). Dorr and Munnich (1989) concluded that migration rates of ^{210}Pb in soils are identical to those of refractory carbon ^{14}C. Pb thus has the potential to be a powerful tracer of soil C dynamics via their shared incorporation into organo-metallic colloids.

Given its fixed association with soil carbon, Pb may arguably be considered a conservative element, forming stable organo-metallic colloid complexes similarly to major elements Fe and Al (Kaste et al., 2011a; Pokrovsky et al., 2005) and refractory trace elements (Thompson et al., 2006; Bern et al., 2015). Insofar as Pb binding to soil solids is functionally permanent on centennial timescales, Pb is a conservative tracer of organo-metallic colloidal phases. ^{210}Pb chronometry can thus describe timescales of critical and poorly constrained processes of organo-metallic colloid transport (Eusterhues et al., 2003; Kalbitz and Kaiser, 2008; Ferro-Vázqeuz et al., 2014), atmospheric carbon sequestration (Dorr and Munnich, 1991; Miller and Friedland, 1994), as well as general soil properties such as rates of podsolization (Steinnes and Friedland, 2005). As a tracer of fundamental soil processes, Pb thus provides a powerful comparator for the behavior of other elements insofar as their convergence with or divergence from the processes traced by Pb (Klaminder and Yoo, 2008). Klaminder et al. (2008) suggested that both Pb and Hg record a temporal record of their deposition in organic rich soil O-horizons. Kaste et al. (2011a) first applied conventional ^{210}Pb chronometry to soils, showing that the well-preserved litter layers of spodosols form by burial in a manner analogous to sedimentation. Whereas Kaste et al. (2011a) found general agreement between ^{210}Pb dates and independent time markers including gasoline Pb isotopic signatures and nuclear bomb-fallout (Warneke et al., 2002), their broad sampling intervals and multi-decadal uncertainties were too coarse to test ^{210}Pb dating in a universal soil context.

Here we test the application of robust ^{210}Pb chronometry to soils. We compare the classic Constant Rate of Supply model (CRS; Appleby and Oldfield, 1978) with a novel one, the Linked Radionuclide aCcumulation model, LRC or "lark", which incorporates processes endemic to soils and omitted from original ^{210}Pb models for sedimentary systems. The LRC model links concurrent measurements of ^{210}Pb and cosmogenic beryllium-7 (half-life 54 days; Huh, 1999; Landis et al., 2012b). ^{7}Be shares both an atmospheric source and depositional characteristics with ^{210}Pb (Baskaran et al., 1993; Landis et al., 2014) and has previously been combined with ^{210}Pb as a chronometer of sediment transport (Matisoff et al., 2005). In soil systems the simultaneous measurement of ^{7}Be and ^{210}Pb via gamma spectrometry accommodates depositional heterogeneity, interception by overlying vegetation, and the rapid penetration of both ^{7}Be and ^{210}Pb into the soil subsurface during their deposition in rainwater. These critical processes are omitted from models adapted for sedimentary systems.

Both LRC and CRS models are empirical and require a conceptual basis for their application to natural systems. Here we develop a conceptual framework for applying atmospheric ^{210}Pb chronometers to soil systems. We begin with a description of the LRC and CRS models, we compare them in a numerical simulation, and we then demonstrate application of the models to sampled soil profiles. Within the framework of the LRC model results, we discuss three prerequisites for robust ^{210}Pb chronometry of soil systems, (i) availability of an independent proxy to quantify the rapid advection of atmospheric ^{210}Pb into soil by wet deposition (ii) establishment of an independent, corroborating time marker for ^{210}Pb vertical migration and (iii) a framework for interpreting ^{210}Pb migration rates in the context of long-term soil-forming processes. Finally, we briefly describe advantages and disadvantages of empirical chronometers versus widely adopted analytical advection–dispersion approaches (e.g., He and Walling, 1997; Bossew and Kirchner, 2004).

2. CONSTANT RATE OF SUPPLY (CRS) MODEL

The conventional ^{210}Pb CRS model is fully described elsewhere (Appleby and Oldfield, 1978; Sanchez-Cabeza et al., 2000; Kaste et al., 2011a). Briefly, the CRS approach uses ^{210}Pb as a proxy for advective processes and exploits radiodecay law as follows:

$$I_z = I_0 e^{-\lambda T} \quad (1)$$

where I_z is the cumulative $^{210}Pb_{xs}$ inventory above depth z, I_0 is the cumulative $^{210}Pb_{xs}$ inventory of the entire profile, λ is the ^{210}Pb decay constant and T is the time required for ^{210}Pb to have migrated from the surface to depth z. Conceptually, during exposure of a system to ^{210}Pb deposition (either with sediment or in rainwater), ^{210}Pb accumulates such that a steady-state ^{210}Pb inventory I_0 develops in the total, integrated system after a time period of 5–10 half-lives, or approximately 100–200 years. Subsequent to this time frame, accretion and radio-decay produce an exponential decline in $^{210}Pb_{xs}$ activity with depth. The $^{210}Pb_{xs}$ inventory I_z below a depth z is equated to the steady-state inventory of the entire profile, I_0 (i.e., time zero), but having decayed over time T since the layer z was exposed to deposition. The age of $^{210}Pb_{xs}$ at depth z, which is the time required for I_0 to decay to I_z, is readily solved from Eq. (1).

$$T = \frac{1}{\lambda} \ln\left(\frac{I_z}{I_0}\right) \quad (2)$$

An implicit assumption in the CRS model is that $^{210}Pb_{xs}$ accumulates only at the surface layer, and that this layer remains isolated from ongoing deposition during subsequent burial. But this is not the case in soil systems, where we know from observations of the short-lived radioisotope ^{7}Be that the deposition of atmospheric elements penetrates the bulk soil medium to depths below the surface (Olsen et al., 1985; Wallbrink and Murray, 1996; Kaste et al., 2011a,b; Landis et al., 2012a). Nuclear fallout, e.g. ^{137}Cs, is similarly observed to display an initial depth penetration in surface soils following its deposition (Matsuda et al., 2015), as do controlled applications of ^{134}Cs and ^{210}Pb tracers (He and Walling, 1997). In a sedimentary context Abril and Gharbi (2012) have referred to this penetration as 'non-ideal deposition'. In a soil context Kaste et al. (2011a) used concurrent measurements of ^{7}Be *qualitatively* to constrain the rainwater-driven penetration of atmospheric aerosols, including ^{210}Pb, into the soil subsurface during deposition, but this critical process was not incorporated explicitly into their CRS age model and its effect on age estimates is thus unknown.

2.1. The Linked Radionuclide aCcumulation model, LRC or "lark

^{7}Be and ^{210}Pb have similar biogeochemical behaviors in the surficial environment. The radionuclides share an atmospheric source (Baskaran et al., 1993; Landis et al., 2014), universal distribution, and high particle-reactivity (Robbins, 1978; You et al., 1989; Benoit, 1995; Taylor et al., 2013; Boschi and Willenbring, 2016). The interception of ^{7}Be and ^{210}Pb is functionally identical, that is, their respective fluxes are highly correlated over the ^{7}Be lifetime of $1/\lambda = 78$ days, and both are sequestered efficiently by both live and dead leaf surfaces (Landis et al., 2014). None of the radionuclides ^{7}Be, ^{210}Pb, (or ^{241}Am or Pu, discussed below) are implicated to a meaningful degree in active biological cycles (Mabit et al., 2014). With soil-to-plant transfer factors $<<10^{-1}$ (Tyler, 2004; Wang et al., 2015; Todorov and Djingova, 2015), their inventory fraction in soil that is translocated to plant matter is $<<0.1\%$, which from a mass-balance perspective is minor. Given the short half-life of ^{7}Be, the likelihood of its behavior diverging from that of ^{210}Pb in surface soils appears to be low. In this instance, ^{7}Be may reasonably be assumed to trace the short-term behavior that characterizes the deposition of ^{210}Pb and similar atmospheric species.

To exploit ^{7}Be as a tracer of ^{210}Pb depositional effects, we combine the two in a new chronometer, the Linked Radionuclide aCcumulation model, LRC, based on their non-steady-state accumulation in surface soils. The accumulation of both ^{7}Be and $^{210}Pb_{xs}$ by a homogeneous reservoir follows the standard law of radionuclide ingrowth: the total radionuclide inventory at any time is a function of depositional flux and radioactive decay. First considering ^{7}Be and $^{210}Pb_{xs}$ independently, the total inventory I_T of each grows over time towards an asymptote of D/λ according to

$$I_T = \frac{D}{\lambda}(1 - e^{-\lambda T}) \quad (3)$$

where I is cumulative inventory, D is depositional flux, λ is decay constant, and T is the time or duration of accumulation, or the exposure age of the medium with respect to the governing depositional processes.

When we consider the distribution of radionuclide inventories in a soil system, a principal complication arises as deposition is instantaneously distributed among multiple, stratified components by processes of (1) interception by any canopy of vegetation and (2) penetration of throughfall into the soil subsurface. The two processes are conceptually equivalent; each canopy and soil component (or 'layer') retains some fraction α of the depositional flux. The fractional flux intercepted by the canopy of vegetation may be described as $\alpha_0 D$; previous work has shown that a full canopy retains as much as $\alpha_0 = 50$–90% of depositional flux (Landis et al., 2012a; Likuku, 2009; Kaste et al., 2011b). As ^{7}Be and ^{210}Pb are highly particle-reactive, when the remaining flux balance penetrates the soil surface, each is progressively stripped from suspension along the flow path in some depth-dependent manner (He and Walling, 1997). The depth distribution of penetration into soil may be described as

$$D_s(i) = \alpha_i D \quad (4)$$

where D is total atmospheric flux, α_i is the depth-dependent interception factor, and D_s is the fractional flux reaching soil at depth i. The depth-dependent soil interception factor α_i for ^{7}Be is widely modeled as an exponential function (Wallbrink and Murray, 1996; He and Walling, 1997; Walling, 2013), with h_0 describing the characteristic length scale or relaxation depth:

$$\alpha_i = e^{-\frac{i}{h_0}} \quad (5)$$

With constant atmospheric flux distributed among all vertically-integrated soil and vegetation components as $\alpha_i D$ such that $\sum \alpha_i = 1$, mass balance is preserved with $\sum I_i = I_T$ and the *cumulative* inventory I_T can be written:

$$I_T(T) = \int_0^T \int_0^n \alpha_i D - \lambda I_i \tag{6}$$

That is, the total radionuclide inventory in the stratified soil-vegetation system is equivalent to the time-integrated inventories of all i components 0 through n, where component 0 is always the uppermost (typically vegetation) component. LRC inventories are thus integrated from vegetation down to the soil layer of interest (whereas CRS inventories are integrated from the layer of interest down to the bottom of the ^{210}Pb depth profile).

Eq. (6) has a familiar solution, i.e., Eq. (3). Thus, for a single radionuclide, if α can be determined for each component, exposure time T can be determined. But α cannot be determined by observations of ^{210}Pb alone: rapid depositional processes are obfuscated by ongoing accumulation and longer-term soil processes. However, because the geochemical and depositional behaviors of ^{7}Be and ^{210}Pb are very similar, we might assume that α is equivalent for ^{7}Be and ^{210}Pb (Landis et al., 2014). In this instance, by constructing two equations simultaneously for ^{7}Be and ^{210}Pb and taking their ratio, α is removed. We thus correct ^{210}Pb$_{xs}$ for rapid depositional processes using the observed, empirical ^{7}Be depth profile. Exposure ages of the stratified unit with respect to ^{210}Pb atmospheric deposition may then be reconstructed by the ratio $R^{Be:Pb}$, that is, by the accumulative (from top-most layer down) inventories of ^{7}Be and ^{210}Pb$_{xs}$ in components 0 to n, according to the following:

$$R^{Be:Pb}_{n,0} = \frac{\sum_n^0 I_i^{Be}}{\sum_n^0 I_i^{Pb}} \approx \frac{D^{Be}}{D^{Pb}} \frac{\lambda_{Pb}}{\lambda_{Be}} \frac{(1 - e^{-\lambda_{Be} T})}{(1 - e^{-\lambda_{Pb} T})} \tag{7}$$

This is the LRC model. The right term in Eq. (7) may be solved iteratively for the time T that yields the experimental ratio $R^{Be:Pb}$, which is calculated arithmetically over each layer depth via the middle term. No curve fitting is required. We thus determine for each sampled depth its exposure time with respect to atmospheric deposition, requiring only knowledge of the relative fluxes of ^{7}Be and ^{210}Pb$_{xs}$, and sampling and measurement of vegetation and the soil medium at appropriate depth intervals. Fluxes may be determined either indirectly from the steady-state inventories of an undisturbed soil column, from a reference site, or by direct measurement of atmospheric deposition over an appropriate period of time (Landis et al., 2014).

3. A CONCEPTUAL MODEL OF RADIONUCLIDE ACCUMULATION IN A VEGETATION–SOIL SYSTEM

Application of the LRC model to a soil system is readily demonstrated using a numerical simulation, parameterized from our observations of ^{7}Be and ^{210}Pb and conceptualized

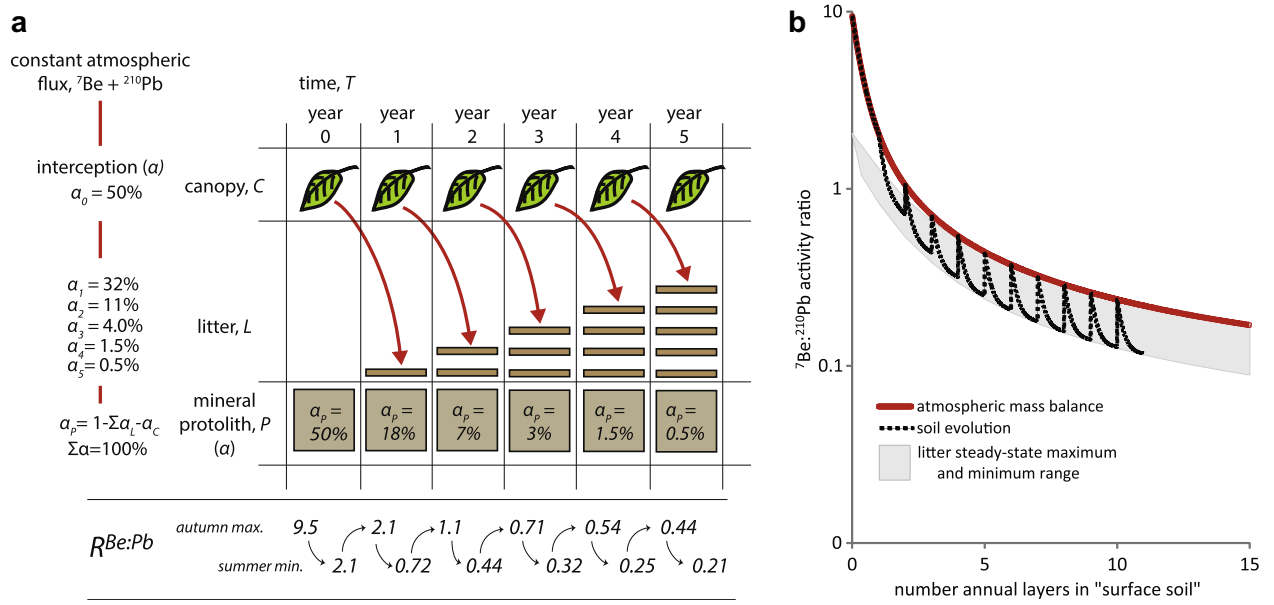

Fig. 1. (a) conceptual model for ^{7}Be and ^{210}Pb accumulation in a soil system, see text Section 3. Daily atmospheric flux is distributed among deciduous canopy, C, and underlying litter, L, or mineral layers, P, with the fraction retained by each described by α, and with $\sum \alpha = 100\%$. Soil is defined as $L + P$. In the bottom panel values of the accumulative inventory ^{7}Be:^{210}Pb$_{xs}$ ratio, $R^{Be:Pb}$, are provided for the autumn maximum and summer minimum of each model year. (b) Model results. The heavy red line represents mass balance, i.e., an 'infinite bucket' in which total atmospheric flux is captured in a single inventory as $L + P + C$. The dashed black line represents soil evolution and only reflects atmospheric mass balance once, in each annual cycle, it has incorporated vegetation following autumnal leaf drop. The shaded gray zone shows the range of litter-only ratios, which describe the steady-state condition for the organic O horizon, and which otherwise share the form and inflection points of 'soil' as a whole.

in Fig. 1. Here we have modeled a deciduous canopy as this proves to be the more dynamic of vegetation systems, though the model is equally relevant to coniferous, perennial, herbaceous or grass-dominated systems. We assume a constant daily ^{7}Be and ^{210}Pb$_{xs}$ flux, that the canopy intercepts 50% of each flux ($\alpha_0 = 0.5$), and that the balance reaches the soil surface as throughfall. (Different parameterizations of interception coefficients do not qualitatively change the model results). We assume that the canopy persists for one year before being incorporated instantaneously, with its radionuclide inventory, into underlying soil as a new litter layer. This new litter layer continues to receive atmospheric deposition over subsequent years but at a diminishing rate that is controlled (shielded) by the superposition of new canopy layers and its burial by subsequent litter layers. The annualized fraction of deposition received by a layer, α, thus diminishes exponentially with time and soil depth (e.g., Eq. (5)). For example, in year one the canopy intercepts 50% of incoming flux ($\alpha_0 = 0.5$), year-old litter intercepts 32% ($\alpha_1 = 0.32$), and the remaining 18% is delivered to the mineral soil. Similarly, during year two, 50% of the incoming flux is intercepted by the canopy ($\alpha_0 = 0.5$), 32% intercepted by the year-old litter layer ($\alpha_1 = 0.32$), 11% is intercepted by the two-year-old litter layer ($\alpha_2 = 0.11$), and the remaining 7% delivered to mineral soil, and so on.

The model described in Fig. 1 allows us to illustrate some critical properties of the atmosphere-soil-radionuclide system, and to demonstrate the mechanics of the LRC model. First, the cumulative ratio $R^{Be:Pb}$ of the soil component (dashed black line in Fig. 1b), is a dynamic property that oscillates seasonally due to overlying vegetation dynamics. It attains an annual maximum value each autumn when the Be-enriched canopy is incorporated as a new litter layer. The soil $R^{Be:Pb}$ ratio then decays towards equilibrium with new, reduced fluxes until the next pulse of ^{7}Be enters with litterfall in the following autumn, an annual cycle that yields pronounced oscillations in $R^{Be:Pb}$. Overall, the oscillating $R^{Be:Pb}$ soil ratio decreases asymptotically as the ^{210}Pb$_{xs}$ inventory grows towards steady-state over many decades. However, if mass balance is achieved by incorporating all superimposed components 0 through n, (i.e., by integrating both canopy and soil inventories), the total inventory ratio $R^{Be:Pb}$ conforms at all times to atmospheric equilibrium and mass-balance via Eq. (3) (red line, Fig. 1b). Thus, $R^{Be:Pb}$, the cumulative ^{7}Be:^{210}Pb ratio of inventories summed over all layers above a given horizon, reflects the atmospheric exposure age of that horizon and forms the basis for a chronometer.

While the fluxes of ^{7}Be and ^{210}Pb$_{xs}$ are distributed to depths in soil identically via the penetration of atmospheric wet deposition, with time the ^{7}Be and ^{210}Pb$_{xs}$ inventory distributions are progressively dislocated as ^{210}Pb$_{xs}$ is buried by litter accumulation and/or translocated downward by colloidal transport. With its short half-life, ^{7}Be does not record these processes. Migration of ^{210}Pb-bearing aerosols and colloids through the soil by organic decay and organometallic colloid dynamics effectively translates the 'layer' of exposure deeper into the surrounding bulk medium, and it is these processes that generate long-lived radionuclide depth profiles that we observe.

For the purposes of quantitative analysis both burial and colloid transport may be considered "advective" processes insofar as each increases the effective distance of a ^{210}Pb-bearing colloid from the soil surface. Our numerical simulation is thus equivalent to the analytical solution offered by Abril and Gharbi (2012) for 'non-ideal' deposition of ^{210}Pb in lacustrine sediments. We compare the two approaches graphically in Fig. 2a. Importantly, by accommodating the depth-penetration of the depositing element, both models reproduce a subsurface ^{210}Pb concentration and inventory maximum that is typical of many soil profiles. This subsurface maximum is, simply put, the result of each 'annual' layer receiving atmospheric deposition for multiple years, albeit at rates that are reduced by its progressive burial. For comparison, depth profiles of ^{7}Be and ^{210}Pb for a real, representative soil profile (details below in Sections 4 and 5) are shown in Fig. 2b and c.

3.1. A test of soil chronometry models using numerical simulation

Applying the CRS age model to our numerical simulation of annually deposited 'layers' (Fig. 1), we show in Fig. 3 that it systematically biases exposure ages too young. The bias results from the penetration of ^{210}Pb to depth during deposition, increasing the Pb inventory in these layers over multiple years. This bias is pronounced (>30% relative error) at the soil surface and diminishes with depth following extinction of the ^{7}Be profile (i.e., at depths below the penetration of deposition). The two models converge for ages more than a few decades old or, equivalently, at depths where ^{7}Be is no longer present. At depths below the occurrence of ^{7}Be, the CRS model is unbiased. For surface layers, by incorporating the ^{7}Be penetration profile, the LRC model in the same scenario returns the correct 'known' age and is thus shown to be unbiased at all depths. This same result is evident when comparing LRC and CRS models for a real, representative soil profile as shown in Fig. 3b. Details on the application of both ^{210}Pb models to real soils are discussed in Sections 5 and 6 below.

4. VALIDATION OF ^{210}PB CHRONOMETRY IN REAL SOILS – AN INDEPENDENT TIME MARKER

While widely used in lacustrine settings, the behavior of nuclear fall-out ^{137}Cs is subject to biological regulation in soil systems (Dupré de Boulois et al., 2008; Steiner et al., 2002; Pietrzak-Flis et al., 1996; Tyler, 2004) and thus its potential to serve as an independent, conservative time marker is compromised. Conversely, plutonium isotopes and the ^{241}Pu daughter americium-241, also products of nuclear bomb testing, appear to be conservative tracers of soil colloid transport. Pu and Am have high valencies of +5/+4 and +3, respectively, are highly particle-reactive, and are mobilized as colloidal complexes (Penrose et al., 1990; Kersting et al., 1999). Size-partitioning of ^{241}Pu and ^{241}Am in soils and surface water are very similar, showing a common behavior related to organic colloidal material

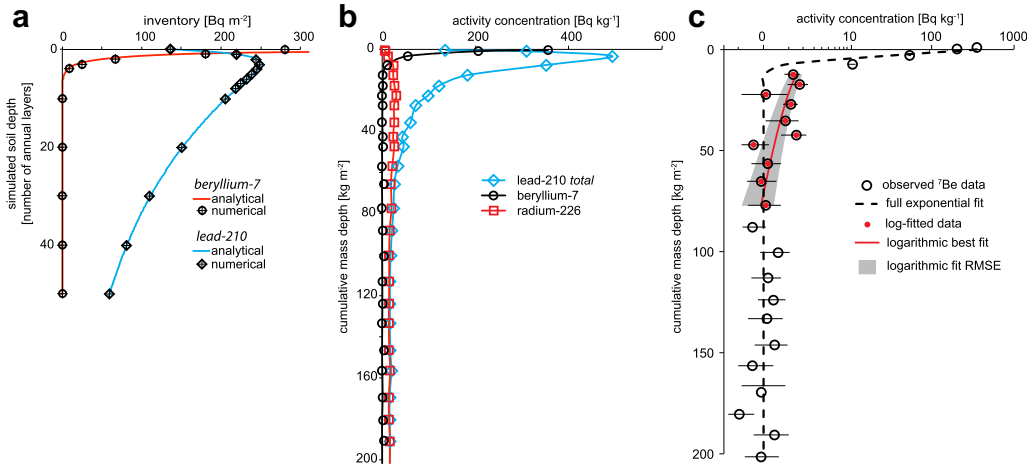

Fig. 2. (a) Numerical simulation of ^{7}Be and ^{210}Pb deposition to an annualized soil numerical model reproduces the analytical derivation of Abril and Gharbi (2012). Both models display a sub-surface peak for ^{210}Pb that results from the depth-penetration of deposition, as indicated by ^{7}Be, integrated over time. (b) Depth profiles for age-model radionuclides for our representative soil profile A6. (c) Close analysis of ^{7}Be depth distribution, with data displayed using log-modulus transform (LM) with LM = sign (^{7}Be)·log(|^{7}Be| + 1). Exponential fit to the full data set is shown with a dashed line. Log-fitted data are shown in closed circles, with line (solid) of best-fit and model RMSE in shading. Error bars show 1-sigma analytical errors.

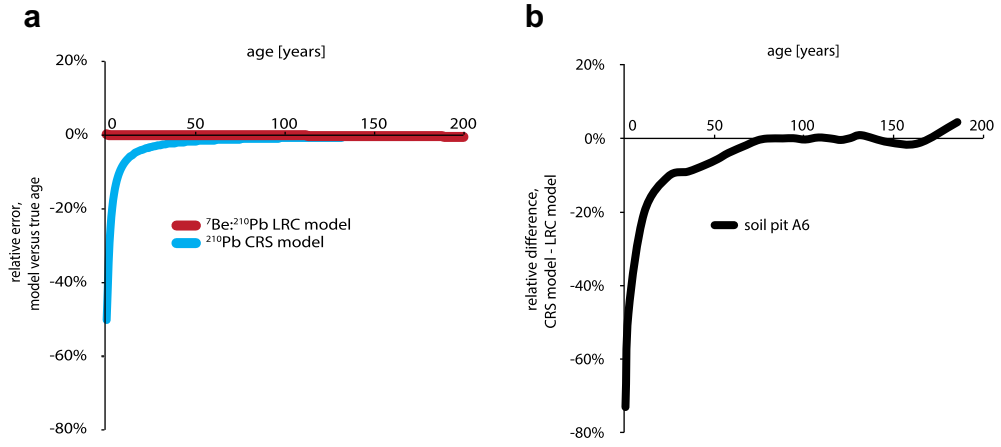

Fig. 3. (a) ^{210}Pb age models applied to our numerical soil model. The CRS model is biased because it does not incorporate depth penetration of ^{210}Pb atmospheric deposition into subsurface soil. The LRC model returns an unbiased age. (b) Relative difference between CRS and LRC models for soil pit A6, which displays the expected bias in CRS model.

(Santschi et al., 2002). Am and Pu mobility in forest soils are virtually identical (Bunzl et al., 1992). Because ^{241}Pu has a relatively short half-life of 14.3 years, the occurrence of ^{241}Am (half-life 432 years) in the natural environment is the result of its ingrowth over several decades following nuclear bomb testing. Thus, behavior inferred from observations of ^{241}Am is some aggregate of the combined ^{241}Pu–^{241}Am system; based on their similar geochemical behaviors, we interpret ^{241}Am as a surrogate for ^{241}Pu depositional and geochemical history. We might expect higher mobility of Pb than Am/Pu, if Pu has entered soils as primary particles of fissile, metallic plutonium, whereas ^{210}Pb enters as ions sorbed or coordinated to sub-micron aerosols (Graustein and Turekian, 1989).

As for ^{137}Cs, a strong peak in atmospheric deposition of ^{241}Pu–^{241}Am is attributed to the years 1963–4 (Warneke et al., 2002; Hirose et al., 2008), though some records show a broad doublet spanning *ca.* 1955 to 1963 (Koide et al., 1977; Olivier et al., 2004; Gabrieli et al., 2011). We assign the ^{241}Pu–^{241}Am depositional maximum to 1963 with a somewhat arbitrary uncertainty of ±3 years in consideration of the variability among different fallout records and in recognition of possible variations in the time required for ^{241}Pu delivered to any canopy of vegetation to have migrated to the ground level. From estimated global ^{239,240}Pu fallout inventories across the latitudinal band 40–50°N (Hardy et al., 1973), ^{239,240}Pu:^{241}Pu isotopic composition of fissile material (Livingston et al., 1975), and the coupled decay-rates of ^{241}Am and ^{241}Pu, we estimate that our location at *ca.* 45°N now hosts a cumulative ^{241}Am inventory of *ca.* 30 Bq m^{-2}. This is near to the maximum ^{241}Am that will occur by ingrowth from ^{241}Pu as the latter is nearly exhausted

by radiodecay. ^{241}Am is now more readily measurable than at any time in the past (Appleby et al., 1991).

It is our expectation that the atmospheric ^{241}Pu depositional maximum of 1963 is approximated by the fixed-depth soil interval with a maximum inventory of ^{241}Am (i.e., Bq m^{-2} cm^{-1}). This 'inventory maximum' is the integral of soil interval concentration (Bq kg^{-1}) versus interval mass (kg m^{-2} cm^{-1}). We use the inventory maximum because activity-concentration (i.e., Bq kg^{-1}) is confounded by dilution into soil materials of differing specific density, e.g. organic matter versus iron oxides. This dilution effect is pronounced in surface soils where density increases rapidly with depth during the transition from organic to mineral horizons.

5. METHODS FOR TESTING ^{210}PB CHRONOMETERS OF SOIL PROCESSES

To test the abilities of both the CRS and LRC models to provide accurate exposure ages of real soils to atmospheric deposition, we sampled three sites at two locations, each with geomorphically stable soil profiles in flat terrain but differing, dominant vegetation. Each site was expected to be 'old' with respect to ^{210}Pb deposition; that is, more than 100 years since soil disturbance. Thus each is expected to have recorded the history of nuclear bomb testing. Soils in our region show minimal physical mixing or bioturbation (Kaste et al., 2007). Consistent with this, each site shows well-developed horizonation. We collected litter and soil samples at level sites on 30 × 30 cm squares, details are described in Supporting Information. Litter horizons were sectioned vertically as fresh or old whole leaves (both Oi horizon), and old leaf fragments (Oe). Underlying humified and mineral horizons were excavated in measured 1 cm depth intervals. All litter and soil samples were bagged quantitatively and in their entirety in the field. In the laboratory, samples were air-dried, sieved at 2 mm to remove coarse roots, wood fragments and stones, and weighed. Subsamples of the <2 mm fraction were then taken by mass, air dried to constant weight, and prepared for measurement of gamma-emitting radionuclides.

Site "A" on the Androscoggin River, New Hampshire, USA, is characterized by sandy loam spodosol soils under mixed hardwood trees and is developed from granite-derived outwash till. Soil pit A6 shows a well-developed E horizon, and was sampled following autumn leaf fall such that the deciduous canopy was recovered at the ground level. Soil pit A1 is of the same soil type but less developed and without a fully developed E horizon. This pit was sampled during autumn leaf fall when some leaf cover remained in the canopy. Our site A1 provides a means for evaluating ^{210}Pb age models relative to Hg contaminant behavior, as this site is adjacent to the Berlin, New Hampshire chlor-alkali Superfund site. The production history of this facility provides constraints on local Hg contamination. Hg electrolysis was implemented at the chlor-alkali facility in the early 20th century (ca. 1908–1937) but was suspended abruptly in 1962 (EPA, 2005). For this site we measured soil total Hg (Hg_T) using a combustion Direct-Mercury-Analyzer (Milestone DMA-80).

Site "M" is located in the Marsh-Billings-Rockefeller National Park, Woodstock, Vermont, USA and characterized by upland coniferous forest on inceptisol soils, also characterized as sandy loam. Here soil pit M2 was sampled under Eastern white pine, and pit M1 was sampled nearby from an adjacent fallow pasture vegetated by perennial grasses. Both soils are developed from thin, loamy till and underlying schist, phyllite and interbedded quartzose limestone of the Waits River Formation. Site M1 is used to derive the local ^{7}Be inventory but is not suitable for explicit ^{210}Pb dating due to its agricultural history. Historically the site has been hayed for fodder, with vegetation and associated ^{210}Pb exported from the site, though it had not been hayed for 3 years prior to sampling.

5.1. Gamma spectrometry and radionuclide measurements

Aliquots of each dry sample were packed into 110 cm^3 polyethylene pucks for gamma counting. All measurement and data processing methods follow Landis et al. (2012b). Gamma instrument calibration was performed using CCRMP (Canadian Certified Reference Material Project, NRC Canada, Ottawa) uranium BL5 and thorium OKA2 ores diluted into matrix soils and sediments similar to those of our samples. Self-attenuation of standard and sample gamma emissions is corrected at all energies (Landis et al., 2012b) using a planar multi-nuclide source and the derivation of Cutshall et al. (1983). Attenuation measurements and their sample mass-dependency are shown in Fig. SI 1; see Shakhashiro and Mabit (2009).

We report the following radionuclides, with the energies of their characteristic gamma emissions: ^{7}Be at 477 keV, with correction for ^{228}Ac at 478 keV (Landis et al., 2012b); ^{210}Pb at 46.6 keV; ^{241}Am at 59.5 keV; ^{234}Th at 63.3 keV with correction for ^{232}Th *via* assumed ^{228}Ra (^{228}Ac) equilibrium; ^{228}Ra via ^{228}Ac at 911 keV; ^{226}Ra at 186 keV with correction for ^{235}U *via* ^{238}U (assuming equilibrium with ^{234}Th; see Dowdall et al., 2004; Zhang et al., 2009). All samples are counted for 4–7 days each to provide adequate precision for ^{241}Am, ^{7}Be at the tail of its depth distribution, and ^{226}Ra in defining 'excess' ^{210}Pb. Cumulative uncertainties are propagated by standard methods and are typically in the 1–5% range; one-sigma uncertainties are provided in all figures and tables. Our analyses of reference materials of a variety of compositions are summarized in Table SI 1.

Measurement of $^{210}Pb_{xs}$ bears some special defining. Atmospheric deposition of ^{210}Pb to surface soils yields total ^{210}Pb activities that exceed those that are supported by *in situ* decay through the (abbreviated) geogenic decay chain ^{226}Ra > ^{222}Rn >> ^{214}Pb > ^{214}Bi >> ^{210}Pb. Here, as is typical, we determine atmospheric or $^{210}Pb_{xs}$ arithmetically by subtracting ^{226}Ra activity (which is a surrogate for 'supported' ^{210}Pb). This often results in 'lead deficiency' at depth. This is expected and attributable to chronic emanation of gaseous radon from soils and sediments (Graustein and Turekian, 1990; Greeman and Rose, 1996; Du and Walling, 2012), the very disequilibrium process that introduces ^{210}Pb to the atmosphere via decay of airborne ^{222}Rn. Where lead deficiency is apparent in 'deep samples', we average the fractional lead deficiency (Pb/Ra < 1)

measured across these deep samples as a correction factor for *in situ* radon loss by multiplication with the measured Ra at all depths. Thus, the supported $^{210}Pb_{supp}$ at any depth i is calculated by multiplication of the ^{210}Pb:^{226}Ra ratio for deep samples (with no atmospheric lead) by the observed ^{226}Ra activity at each depth:

$$[^{210}Pb_{supp}]_i = \frac{[^{210}Pb]_z}{[^{226}Ra]_z}[^{226}Ra]_i \quad (8)$$

where $^{210}Pb_{supp}$ is the activity of ^{210}Pb which is supported by *in situ* radioactive decay of ^{226}Ra via ^{222}Rn at any depth i, and z denotes depths below the $^{210}Pb_{xs}$ atmospheric cap. This method is similar to defining a ^{210}Pb asymptote to estimate $[^{210}Pb_{supp}]_i$ (Matisoff, 2014), but improved in that the correction accounts for changing Ra activity with depth (see Figs. 2b and SI 2). Our implied assumption that fractional radon losses through emanation are constant with depth is not correct (Davidson and Trumbore, 1995), but as a first approximation is reasonable given analytical uncertainties in ^{210}Pb and ^{226}Ra measurements and the vast difficulty in knowing the true, long-term average Rn loss from soils *in situ*. For site A1 we did not collect 'deep' samples from which we might estimate chronic Rn losses, so we assume identical radon losses as for the nearby A6 site ($^{210}Pb_z$:$^{226}Ra_z = 0.97 \pm 0.06$, Table 1). For site M2, Rn disequilibrium was estimated as 0.80 ± 0.05. As others have pointed out (Kaste et al., 2011a), the effect of ^{222}Rn loss is minor relative to the orders-of-magnitude higher atmospheric ^{210}Pb in surface soils (Fig. 2b). But the error in calculating cumulative ^{210}Pb inventory is comparable (*ca.* 5%) to our analytical uncertainties and thus warranting of attention in our effort to produce the most accurate age model.

6. RADIONUCLIDE MEASUREMENT RESULTS

Radionuclide measurements are summarized in Table 1 and detailed in Table SI 2. Both ^{7}Be and ^{210}Pb measured inventories agree well with direct measurement of depositional fluxes monitored at Hanover, NH (Landis et al., 2014). Greater than half of the ^{7}Be inventory is stored in vegetation. Throughfall flux of ^{7}Be reaching the soil surface is distributed to subsurface depths in approximately exponential fashion, with relaxation depths, h_0, for our sites A1, A6, M1 and M2 modeled as 1.25, 1.21, 0.86, 1.25 kg m^{-2}, respectively. If we consider only the distribution of ^{7}Be measured in soil, omitting litter, values of h_0 are 3.24, 2.67, 1.84, 1.29 kg m^{-2}. Values for h_0 calculated in the latter manner distinguish sites from one another, and demonstrate the effect of soil properties on ^{7}Be depth penetration: organic litter plays a dominant role in regulating ^{7}Be delivery to underlying soil, where its penetration is controlled by bulk density of the soil column (0.47, 0.52, 0.73, 0.86 g cm^{-3}, respectively; correlation of bulk density with h_0 gives $r^2 = 0.98$). Descriptive parameters for ^{7}Be depth distributions are summarized in Table 2. Non-exponential tailing is evident in each of the ^{7}Be depth distributions; our logarithmic fitting to these tails are shown in Figs. 2c and SI 3 and described in Supporting Information.

Total ^{241}Am inventories are in agreement among our sites, and all conform to expectation for global bomb-testing flux, which we have estimated in Section 4 at *ca.* 30 Bq m^{-2}. Our site inventories average 28.8 $\pm$ 1.8 Bq m^{-2} (mean $\pm$ 1σ standard deviation, Table 1). Among soil profiles the ^{241}Am inventory maximum, or equivalently the concentration-mass depth integral maximum, varies in depth from 2.5 to 6.0 cm. Depth profiles are illustrated in Fig. 4. ^{137}Cs inventories and depth profiles are similarly shown in Fig. 5. ^{137}Cs inventories are consistent among the sites, but we did not capture the full inventory at two of our soil pits due to pronounced tailing of ^{137}Cs with depth. Inventories at sites A1 and A6 are $>1473 \pm 29$ and $>1301 \pm 25$ Bq m^{-2}, respectively. At site M2 we appear to have recovered the total ^{137}Cs inventory and we estimate it to be 1678 ± 33 Bq m^{-2}. These values are consistent with regional estimates of total ^{137}Cs deposition from the Nevada Test Site and global weapons testing provided by Simon et al. (2004); our interpolation of their data yields an estimate of total fallout, decay-corrected to the time of our sampling, of 1550 ± 300 Bq m^{-2}.

7. ^{7}BE-^{210}PB CHRONOMETRY AND INSIGHTS INTO MODERN SOIL PROCESSES

Details of chronometer construction are given in Supporting Information. In Fig. 4 we show LRC and CRS results and their analytical confidence intervals, superimposed on ^{241}Am depth distributions. LRC age estimates for the ^{241}Am maxima of the three soils fall within analytical uncertainties of the presumed age, averaging 1967 ± 5 (calendar year $\pm$1 standard deviation). Individual ages are 1972 ± 3, 1962 ± 3, 1967 ± 4 for the A1, A6 and M2 sites. CRS ages average 1972 ± 4 (Table 1). As expected, divergence between the two ^{210}Pb age models is small at the bomb fallout age of 50 years, but the bias toward younger exposure ages we anticipate in the CRS model, based on numerical modeling, is present. The LRC and CRS models diverge to an extent determined by the ^{7}Be depth distribution relative to that of the ^{210}Pb distribution. Where the CRS model becomes unbiased, uncertainties for the LRC model explode as the accumulative $R^{Be:Pb}$ ratio can no longer be analytically resolved from its asymptote. ^{137}Cs inventory maxima are significantly younger than expected for bomb testing, averaging 1988 ± 8 years.

Close agreement between the LRC model and ^{241}Am bomb-fallout demonstrates that Pb and Am/Pu behavior is congruent in these soil systems. Despite locations of the ^{241}Am bomb fallout horizon at disparate depths in different horizons among various soil profiles, ^{210}Pb chronometry shows that these depths in each case correspond to a narrow span of time consistent with the peak of nuclear bomb testing. Far beyond a coincidence of their co-location in surface soils, ^{210}Pb and ^{241}Am are correlated to a precise degree by the exact distributions of their respective inventories. Similarly, we find congruence of ^{210}Pb with Hg_T behavior at our A1 site (Fig. 6), which was contaminated with *ca.* 29 g m^{-2} total Hg or approximately 10$\times$ more than background contamination expected from long-range transport sources. A very sharp, truncated peak in the Hg depth profile corresponds to a depositional age of 1967 $\pm$ 3 years via the LRC model, which is consistent with

Table 1
Radionuclide inventories and chronometry parameters for soil exposure dating by LRC and CRS models.

	Site	A1		A6		M2		M1[d]	
	Canopy	Beech, oak		Beech, oak		White pine		Perennial grass	
	Vegetation	Forest		Forest		Forest		Pasture	
	Soil	Spodosol		Spodosol		Inceptisol		Inceptisol	
	Sampling date	25-09-2014		07-11-2014		13-11-2014		13-11-2014	
		Parameter	σ	Parameter	σ	Parameter	σ	Parameter	σ
^{7}Be	Soil inventory [Bq m^{-2}]	187	9	440	14	185	9	159	12
	Canopy inventory [Bq m^{-2}]	*238*[a]	10	*n/a*		*195*[b]	12	221	6
	Measured total	*n/a*		440	14	*380*[b]	8	379	9
	Regional total[c]	427	5	445	5	415	5	415	5
	Empirical site flux [Bq m^{-2} y^{-1}]	2004	25	2062	67	1777	42	1777	42
	Canopy interception	56%		*n/a*		55%		58%	
$^{210}Pb_{excess}$	Soil inventory [Bq m^{-2}]	5193	109	5703	90	5215	109	>3466[d]	127
	Canopy inventory [Bq m^{-2}]	83[e]	5	*n/a*		122[f]	9	161	5
	Empirical site flux [Bq m^{-2} y^{-1}]	164	3	177	3	166	3	*n/a*	
	Empirical Be:Pb flux ratio	12.2	0.3	11.6	0.2	10.7	0.3	*n/a*	
	Disequilibrium coefficient, ^{210}Pb:^{226}Ra	*n/a*	*n/a*	0.97	0.06	0.80	0.05	0.81	0.03
^{241}Am	Soil inventory [Bq m^{-2}]	28.1	2.3	27.5	2.5	30.9	2.3	29.9	3.2
	Regional prediction [Bq m^{-2}]	*30*		*30*		*30*		*30*	
	$R^{Be:Pb}$ inventory maximum [calendar year]	*1972*	*3*	*1962*	*3*	*1967*	*4*	*n/a*	
	CRS inventory maximum [calendar year]	*1975*	*2*	*1967*	*2*	*1970*	*3*	*n/a*	
^{137}Cs	Soil inventory [Bq m^{-2}]	>1437	29	>1301	25	1678	33	>1338	49
	Regional prediction [Bq m^{-2}]	*1550*	*300*	*1550*	*300*	*1550*	*300*	*1550*	*300*
	$R^{Be:Pb}$ inventory maximum [calendar year]	*1983*	*2*	*1997*	*1*	*1983*	*3*	*n/a*	

[a] Canopy ^{7}Be is inferred by mass balance using regional reference site inventory Landis et al. (2014).
[b] Canopy ^{7}Be is inferred from total inventory measured at adjacent reference location M1.
[c] Total inventory recorded at regional reference Hanover, NH as of soil sampling date Landis et al. (2014).
[d] Site M1 is agricultural and is periodically hayed for fodder, exporting ^{210}Pb inventory in vegetation; the site had not been hayed for 3 years prior to sampling so ^{7}Be inventory is intact.
[e] Canopy ^{210}Pb is inferred from fraction ^{7}Be inventory in canopy and ^{7}Be:^{210}Pb flux ratio.
[f] Canopy ^{210}Pb is inferred from fraction ^{7}Be inventory in canopy, ^{7}Be:^{210}Pb flux ratio, and an assumed canopy turnover time of 1.5 years typical for *Pinus strobus*.

Table 2
Descriptive parameters for ^{7}Be depth distribution in soils.

Parameter		Site			
		A1	*A6*	*M2*	*M1*
Litter mass	[kg m^{-2}]	0.90	0.90	1.54	0.62
h_0, soil-plus-litter[a]	[kg m^{-2}]	1.25	1.21	1.25	0.86
h_0, soil only[b]	[kg m^{-2}]	3.20	2.70	1.30	1.84
^{7}Be 'zero' depth[c]	[kg m^{-2}]	67.5	71.3	59.4	69.8
^{7}Be 'zero' depth[c]	[cm]	7.5	10	7	9.5
^{7}Be soil density[d]	[g cm^{-3}]	0.47	0.52	0.86	0.73

[a] h_0 is fit using $I(z) = \exp(z/h_0)$, i.e., Eq. (5).
[b] Exponential function is fit to humified soil intervals only, litter omitted.
[c] Estimated from log-fit of the observed depth profile tail.
[d] Bulk density for the soil column containing ^{7}Be.

abrupt decommissioning of the facility in 1962 (EPA, 2005). Net Hg migration rates of 0.8 mm yr^{-1} measured here for our A1 site are similar to those shown for atmospheric Hg migration by Jiskra et al. (2015) using stable Hg isotopic measurements.

We contend that the convergence in behavior among ^{210}Pb, ^{241}Am and Hg_T is attributable to their common incorporation into universal soil processes. Pb and Am behavior is known to be colloidally mediated. With respect to Hg, both it and Pb are retained within the soil system largely through their association with soil organic matter (Klaminder et al., 2008; Demers et al., 2013). Pb and Hg, together with Fe and Al are the strongest humate-forming metals (Kerndorff and Schnitzer, 1980). We thus propose that ^{210}Pb migration traces soil colloid processes via mechanisms of (i) regulation of multivalent metal speciation by organic matter (e.g., humics) throughout the pH range of typical soils (Takahashi et al., 1999; Kerndorff and Schnitzer, 1980), (ii) regulation of the solubility of these metal-organic complexes by saturation with Fe and Al (e.g., Ferro-Vázqeuz et al., 2014), (iii) stability of these complexes during both chemical weathering (Bern et al., 2015) and aqueous transport (Pokrovsky et al., 2005).

Observed ^{210}Pb migration rates, on the order of 1–1.5 mm yr^{-1} under deciduous litter and 0.3–0.4 mm yr^{-1} under coniferous litter, are lower as expected under coniferous vegetation where decomposition rates are slower. For both sites A6 and M2 the age models show a convex shape (Fig. 4) that indicates accelerating colloid transport with distance from the soil surface. We interpret this to reflect processes of organic litter decay and liberation of mobile C. The age model profile for site A1 is more heavily influenced by depositional processes, reflected in both deep ^{7}Be penetration and a broadened ^{210}Pb peak (Fig. SI 2). For spodosol A6 the specific role of horizonation in driving colloid transport becomes very apparent. Here ^{210}Pb migration increases from *ca.* 0.5 mm yr^{-1} in Oa horizon, where it is likely to be limited by organic decomposition of leaf matter, to 2.5 mm yr^{-1} through E horizon where eluvial processes are active, before slowing to less than 0.5 mm yr^{-1} in B horizon where accumulation is evident (and a minor accumulation of ^{241}Am is also found, Fig. 4b).

7.1. Development of atmospheric element depth profiles

This critical conclusion may be drawn from ^{210}Pb chronometer results with respect to colloid-metal dynamics: the shape of metal concentration distributions and their position in the soil profile is a product of time and dynamic soil process rates, rather than of static soil properties. As demonstrated with ^{7}Be as proxy, the instantaneous atmospheric deposition of particle-reactive elements to the soil system establishes an inventory maximum at the soil/litter surface with an exponential-like decline below. Following the addition of a conservative tracer pulse, such as ^{241}Am from bomb-testing, the depositional maximum is preserved at (approximately) the layer of deposition even under the progressive action of advective-dispersive processes. In a soil system and $^{210}Pb_{xs}$ context, the layer of deposition must be interpreted as a population of mobile organo-metallic complexes or their precursors. Over time, advective–dispersive processes transform the initial exponential distribution into a peak shape that is approximately Gaussian, tailing to the bottom as a consequence of the initial exponential distribution of depth penetration, while truncated to top by the boundary condition imposed by the soil surface. Only changing rates of advection/dispersion with depth, anisotropy, or more complex (biological) processes further distort the concentration-mass depth peak shape. Our observed ^{241}Am peak shapes conform to the expectation of an idealized depositional peak, as is apparent in Fig. 4.

Conversely, ^{137}Cs peak shapes are irregular or distorted (Fig. 5). ^{137}Cs inventory maxima are significantly younger than expected for bomb testing, indicating discord between Pb/Am/Hg and Cs behavior. The difference in Cs profiles between sites A1 and A6 is remarkable, A1 with a broadly symmetrical shape and A6 with a very pronounced near-surface maximum. These soils share both common parent material and canopy cover, but A1 lacks development of a strongly eluviated horizon. While focusing (or retarding) processes maintain a sharp surface peak in A6, the broad, diffusive ^{137}Cs tail below (Rosén et al., 1999), indicates that these processes are 'leaky'. Cs that escapes the organic horizons is rapidly moved through the soil profile. These characteristics are consistent with the interpretation that surficial focusing is related to biological cycles, which may be leaky due to seasonality in the life cycle of microbial

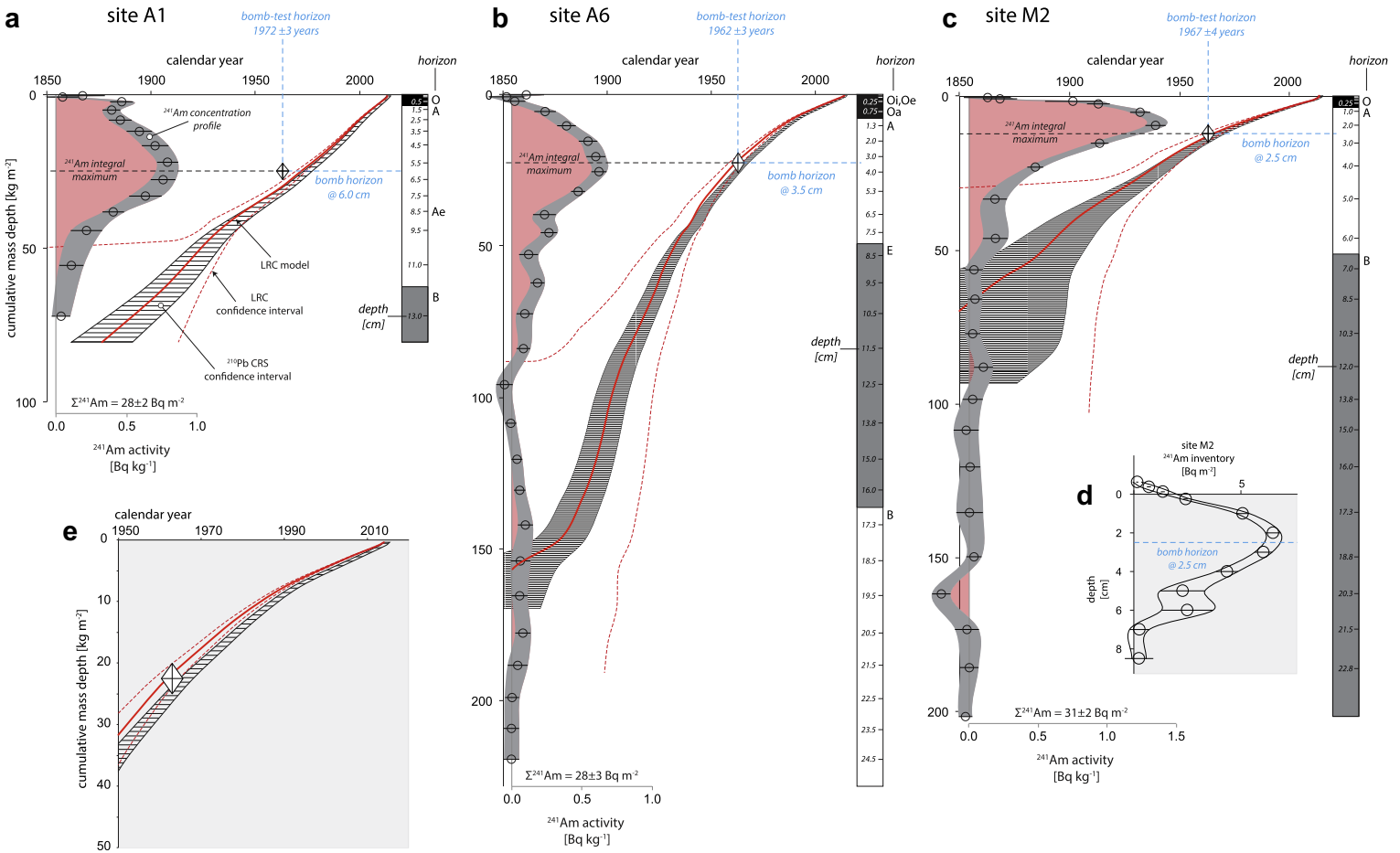

Fig. 4. Soil age-depth models, with americium-241 depth distributions superimposed, for three sites, (a) site A1, an immature spodosol under deciduous maple-beech-birch canopy, (b) site A6, a mature spodosol under same canopy, and (c) site M2, inceptisol under coniferous white pine canopy. The LRC model is shown with 1-sigma confidence intervals (thin dotted lines). The CRS model is represented as its 1-sigma confidence interval in black hatching. ^{241}Am measurements are shown with 1-sigma confidence interval in dark gray, and integrated inventory in red shading. Our assigned peak in ^{241}Am inventory, which we attribute to maximum bomb testing of 1963, is shown by the white diamond. Uncertainties are taken to be ± one-half depth interval and ±3 years, respectively. Inset (d) shows inventory versus depth for site M2, where concentration maximum does not correspond to inventory maximum due to density change through the profile. Inset (e) shows LRC and CRS models for recent decades where divergence of the models is most significant.

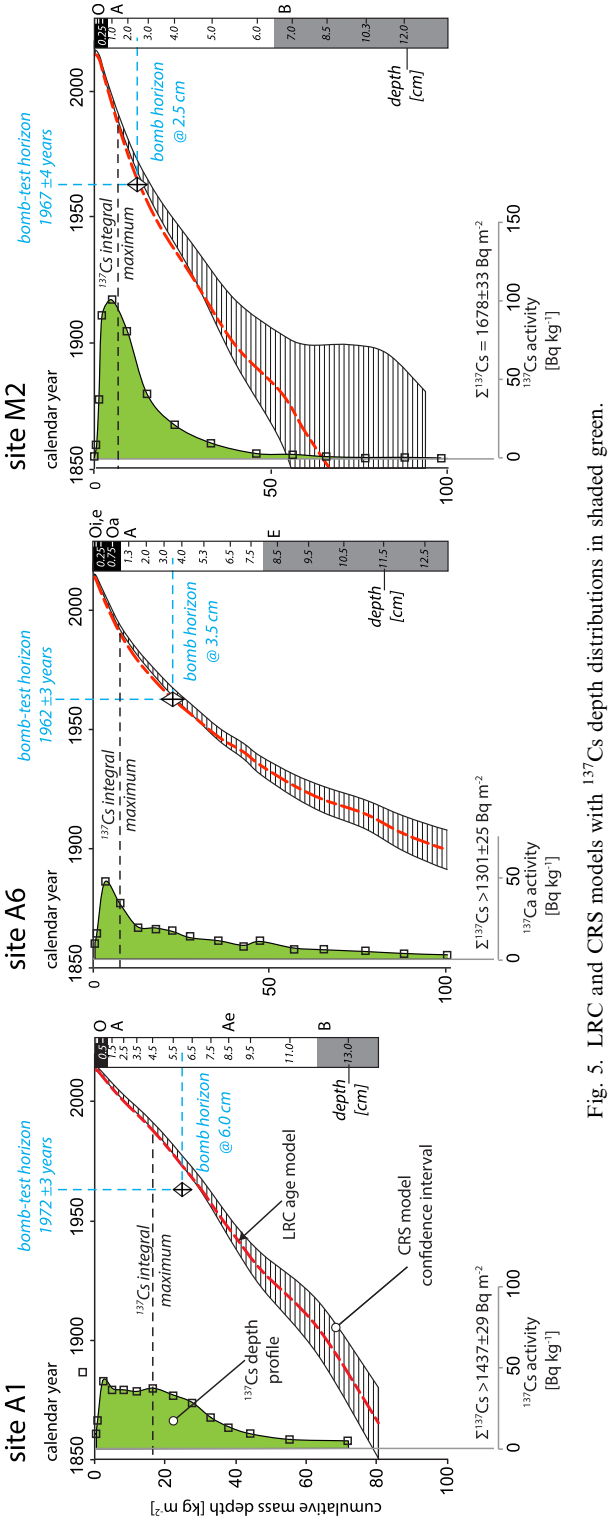

Fig. 5. LRC and CRS models with ^{137}Cs depth distributions in shaded green.

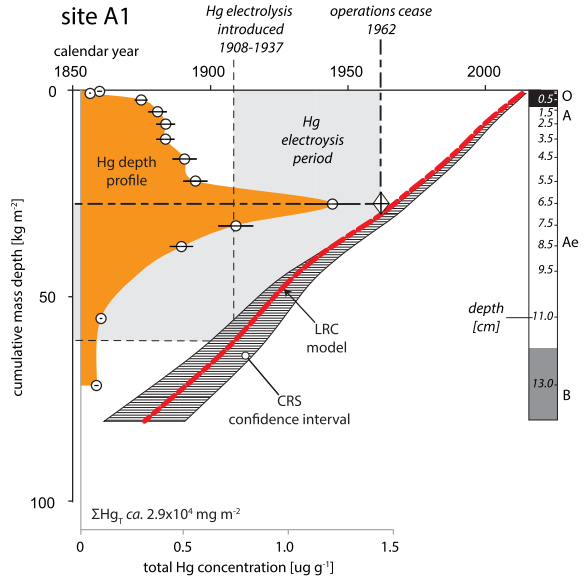

Fig. 6. LRC and CRS age models and total Hg profile for site A1, which was contaminated with Hg from the Berlin, NH chlor-alkali Superfund site. Hg electrolysis began in 1908–1937 but ended abruptly in 1962 (EPA, 2005). Remediation of the facility began in 1999–2000.

communities and soil solution chemistry (Zabowski and Ugolini, 1990; Pietrzak-Flis et al., 1996; Kaiser et al., 2001; Landis et al., 2012a). Consequently, ^{137}Cs does very little for soil chronometry in our organic-rich, clay-poor soils (see Sanchez et al., 1999), though it may be useful as an indicator of, for example, fungal activity or nutrient stress. ^{210}Pb thus provides a powerful comparator for other elements whose behavior, like that of Cs, may not be controlled by colloidal processes to the same extent as Pb, or may be regulated by other processes altogether.

7.2. Advantages and limitations of ^{210}Pb empirical chronometers

The migration of metals through soil profiles is traditionally described using analytical advection–dispersion models (e.g., Dorr and Munnich, 1991; He and Walling, 1997; Bossew and Kirchner, 2004). Versus these approaches LRC modelling provides critical advantages of (i) explicit and quantitative incorporation of atmospheric depositional processes for each soil profile, (ii) depositional processes calibrated *in situ* using simultaneous ^{7}Be measurements, with no assumptions regarding functionality of the atmospheric deposition depth penetration, (iii) calculation of migration rates that are depth dependent and require no assumptions about the number or nature of governing soil processes. Incorporation of the ^{7}Be depositional profile into the LRC model explicitly accommodates the short-term redistribution of radionuclide contaminants following their introduction to soil, as from the Chernobyl or Fukushima disasters, where advection–dispersion modeling has not been successful (Bossew and Kirchner, 2004). We are

similarly able to resolve a fundamental question regarding the shape of the Pb depth profile, namely, its subsurface peak. Whereas Friedland et al. (1984) and Grondin et al. (1995) suggested specific sorption affinity of organic soil layers, Kaste et al. (2011a,b) invoked its concentration by organic decay and CO_2 loss, and Klaminder et al. (2008) warned about conflating this feature with the historical pattern of atmospheric deposition, here we demonstrate that for ^{210}Pb, its continuous deposition via rainwater percolation alone can produce this feature.

It must be stressed here that the ^{210}Pb age models do not represent a history of the atmospheric deposition *per se*. The LRC and CRS models describe *net* transfer, or advection, such that we are able to date only the *inventory maximum* of a contaminant pulse as shown here with ^{241}Am. Total transport rates are compounded when dispersive processes act in concert with accelerating advection, such that a significant fraction of the total ^{241}Am inventory may be found quite deep in the profile where ^{210}Pb models produce ages many decades older than the advent of fissile plutonium (and americium). For the case of nuclear bomb fallout and ^{241}Am, its prolonged period of deposition (*ca.* 1945–1975) introduces a dispersion-like effect to the initial soil profile condition and, consequently, we cannot make a reasonable assessment of *in situ* dispersive process rates. Only with estimates of dispersion can a true depositional history be reconstructed. In the future this might be accomplished through a hybrid approach, by inverting a complete advection–dispersion model with known, depth-dependent rates, which are calibrated by an empirical age model such as the LRC model described here.

As for sedimentary systems, in soil systems ^{210}Pb dating provides high-precision process rate estimates, with uncertainties in the 3–5% percent range for up to 30-year timeframes by means of the LRC model. LRC uncertainties explode as the accumulative ratio $R^{Be:Pb}$ approaches its asymptote, but here the 'non-ideal deposition' bias in conventional ^{210}Pb CRS modeling becomes trivial. In this timeframe the CRS model offers analytical precision on the order of 5% for the range 30–100 years. The two ^{210}Pb age models should thus be seen as complementary, with the incorporation of ^{7}Be required where it is present and allowing us to discount the effects of rapid rainwater percolation where it is absent. Simply put, the presence of ^{7}Be at depth in a soil forces us to reinterpret the mechanisms and rates by which co-occurring ^{210}Pb arrived at those same depths.

8. BROADER APPLICATIONS OF SOIL ^{210}PB CHRONOMETRY

Through their efficient accumulation in vegetation, it is well established that both the ^{7}Be and ^{210}Pb tracers, as well as pollutants including Pb, Hg (Demers et al., 2013), nuclear fallout ^{137}Cs (Kato et al., 2012), and a number of other metals such as Se (Blazina et al., 2014) or Zn, Cd, Mo and W (Steinnes and Friedland, 2006) are introduced to soil systems via atmospheric deposition. Our tracing of the post-depositional migration of atmospheric metals using LRC and CRS models is validated here with ^{241}Am bomb fallout and is consistent with that of local Hg contamination, leading us to propose that ^{210}Pb chronometry is a valuable tool for quantifying modern soil processes and the incorporation of atmospheric elements into soil systems. Application of $^{210}Pb_{xs}$ models to other metals and soil conditions requires careful consideration of, e.g., metal speciation, pH, active biological uptake, or redox cycles, which may cause them to diverge from the conservative colloid migration that typifies Pb and Am in our model soils. Here we emphasize that ^{210}Pb chronometry of soil systems is both conceptually valid and valuable, provided a proper interpretation of model results. Exposure aging derived from these models are not interpretable with reference to the soil bulk medium, but instead provide insight into the mechanisms and rates by which atmospheric elements are processed through the soil system. Lacking specific tracers for each element of interest, atmospheric ^{210}Pb behavior thus provides us with a metric of *in situ* universal processes, such as litter decomposition and colloid migration, between sites and sampling times, from which we may interpret the relative behaviors of other elements.

The potential of ^{210}Pb dynamics to inform us about soil processes is enormous, but ^{210}Pb chronometry of soils (with ^{241}Am corroboration) faces the same challenges that have been found in sedimentary systems. These include difficulties in validating steady-state assumptions and post-depositional mobility, in corroborating independent time markers (Davis et al., 1984), violations of radioactive equilibrium underlying ^{210}Pb production from the uranium decay series both *in situ* (Imboden and Stiller, 1982; Du and Walling, 2012) and during analysis (Zhang et al., 2009), and analytical complications regarding the direct measurement of both ^{210}Pb (Shakhashiro and Mabit, 2009; Mabit et al., 2014) and ^{7}Be (Landis et al., 2012a,b). With respect to soil systems we add complications of differential elemental behavior in the context of multiple, poorly constrained soil processes (Matisoff et al., 2011; Demirkanli et al., 2009). The dynamic nature of ^{7}Be deposition and its representation of historical ^{210}Pb deposition must also be considered (see Appendix). Nonetheless, with appropriate attention to these challenges, ^{210}Pb dating remains a primary means for reconstructing contaminant deposition in sedimentary systems (Appleby, 2001; Mabit et al., 2014; Matisoff, 2014) and will prove invaluable, as well, in soil systems. Finally, the LRC method may complement dating of sedimentary systems, too, where ^{7}Be may be found to some depth in surface sediments (e.g., Santschi et al., 1999) and peat (Hansson et al., 2014). Here ^{7}Be can correct ^{210}Pb for this 'non-ideal deposition' (Abril and Gharbi, 2012) in the same manner that we have used it for rainwater depositional processes in soils.

ACKNOWLEDGEMENTS

Soils in the Marsh-Billings-Rockefeller National Park were collected under permit – special thanks to K. Jones for his assistance in accessing these sites. Thanks also to B.P. Jackson and the Dartmouth Trace Element Analysis Core facility for providing Hg measurements with support from NIEHS P42ES007373.

APPENDIX 1.

A1. Dynamic nature of ^{7}Be occurrence and limitations of the LRC model

In the Linked Radionuclide aCcumulation model (LRC) we assume that the ^{7}Be depth profile observed in soils reflects long-term, average behavior of ^{210}Pb. This assumption requires attention. Walling (2013) has warned that the depth distribution of ^{7}Be is dynamic, and we must consider that variation in, for example, median activity depth h_0, has the potential to influence age determination. It stands to reason that depth penetration may be related to rainfall rate and/or total flux. If so, seasonal differences between ^{7}Be and ^{210}Pb deposition may become problematic due to the combined effects of two phenomena: (i) At our location, ^{210}Pb flux shows a roughly 2× increase in summer over winter, whereas ^{7}Be shows a roughly 8× increase (Landis et al., 2014). The bias to ^{7}Be flux is attributed to seasonal thinning or increasing altitude of the tropopause (Feely et al., 1989), which allows precipitation to nucleate at higher altitudes where ^{7}Be production is greater. (ii) Convective storms characteristic of summer often generate high-intensity and abundant rainfall. Combined, these processes could bias deposition characteristics between ^{7}Be and ^{210}Pb and lead us to overestimate the depth penetration of ^{210}Pb. A similar bias might be present in mountainous regions where 'occult' deposition of ^{210}Pb from cloud water may not be accompanied by equal amounts of ^{7}Be (Stankwitz et al., 2012).

To our knowledge the best data available on ^{7}Be depths in soil are provided by Walling et al., 2009. These authors performed repeat sampling of bare soil in a cleared forest site through the dry-to-wet seasonal transition in southern Chile. The depth distribution of ^{7}Be does change shape in response to rainfall amount, deepening from dry to wet season. There appears to be no systematic relationship between total inventory and h_0, however. Instead, ^{7}Be median depth deepens in the profile as the rainy season progresses. It may be that prior or antecedent wetting of the soil enhances infiltration in wet versus extended dry periods, or that penetration of ^{7}Be into the soil is a multi-step process with some compounding contribution from repeated depositional events. For all observations the gross ^{7}Be depth distribution was well-approximated by an exponential function. Observed values of h_0 range 1.3 to 2.2 kg m^{-2}, with a median of 1.85 ± 0.29. We performed a sensitivity analysis for our A6 site based on this variation, for simplicity assuming a strictly exponential distribution of ^{7}Be with depth. We find that a corresponding $\pm 1\sigma$ error in h_0 translates to errors in age estimation of ±0.6 years at 10 years old and ±0.01 years at 30 years. Because the bomb-test horizon lies below the observed ^{7}Be distribution, its age estimation is not meaningfully affected. The effect on litter age is more pronounced, ±0.15 years at 1 year old or 15% relative.

With neither canopy of vegetation nor leaf litter layers to intercept precipitation and moderate its fall to the ground, the case reported by Walling et al. (2009) is likely an extreme scenario since both ^{7}Be and ^{210}Pb are efficiently scavenged where vegetation and litter are present. The similarity in h_0 reported by many authors, as reported by Walling (2013), gives us confidence that the geochemical nature of ^{7}Be interactions with soil media, rather than weather conditions, dominates its depositional characteristics. It must also be emphasized that the principle factor controlling both ^{7}Be and ^{210}Pb fluxes is rainfall amount (Landis et al., 2014), and because these fluxes are correlated and conform to a law of averaging, both ^{7}Be and ^{210}Pb penetration into the soil should be expected to respond similarly to variations in depositional character. Furthermore, intense rainfall usually generates runoff or pooling rather than percolating further or faster: infiltration rates during intense storms are limiting. We thus expect that the primary challenge to determining a representative ^{7}Be depth profile is related to extreme seasonality in precipitation and related soil moisture characteristics. In all cases, ultimately we would like to know the 'flux-weighted mean' depth penetration of both ^{7}Be and ^{210}Pb. While additional research and site-specific evaluation will be required to develop sampling strategies that best achieve this goal, our present results confirm that including ^{7}Be in a ^{210}Pb age model provides a more accurate estimate of soil process rates.

APPENDIX B. SUPPLEMENTARY DATA

Supplementary data associated with this article can be found, in the online version, at http://dx.doi.org/10.1016/j.gca.2016.02.013.

REFERENCES

Abril J. M. and Gharbi F. (2012) Radiometric dating of recent sediments: beyond the boundary conditions. *J. Paleolimnol.* **48**, 449–460.

Appleby P. G. (2001) Chronostratigraphic techniques in recent sediments. In *Tracking Environmental Change Using Lake Sediments. Volume 1: Basin Analysis, Coring, and Chronological Techniques*. pp. 171–203.

Appleby P. G. and Oldfield F. (1978) The calculation of lead-210 dates assuming a constant rate of supply of unsupported ^{210}Pb to the sediment. *Catena* **5**, 1–8.

Appleby P. G., Richardson N. and Nolan P. J. (1991) ^{241}Am dating of lake sediments. *Hydrobiologia* **214**, 35–42.

Baskaran M., Coleman C. H. and Santschi P. H. (1993) Atmospheric depositional fluxes of Be-7 and Pb-210 at Galveston and College-Station. *Texas. J. Geophys. Res.* **98**, 20555–20571. http://dx.doi.org/10.1029/93JD02182/full.

Beal S. A., Kelly M. A., Stroup J. S., Jackson B. P., Lowell T. V. and Tapia P. M. (2014) Natural and anthropogenic variations in atmospheric mercury deposition during the Holocene near Quelcaya Ice Cap, Peru. *Global Biogeochem. Cycles* **28**, 437–450.

Benoit G. (1995) Evidence of the particle concentration effect for lead and other metals in fresh waters based on ultraclean technique analyses. *Geochim. Cosmochim. Acta* **59**, 2677–2687.

Bern C. R., Thompson A. and Chadwick O. A. (2015) Quantification of colloidal and aqueous element transfer in soils: the dual-phase mass balance model. *Geochim. Cosmochim. Acta* **151**, 1–18.

Blazina T., Sun Y., Voeglin A., Lenz M., Berg M. and Winkel L. H. E. (2014) Terrestrial selenium distribution in China is potentially linked to monsoonal climate. *Nat. Commun.* **5**, 4717. http://dx.doi.org/10.1038/ncomms5717.

Boschi V. and Willenbring J. (2016) The effect of pH, organic ligand chemistry and mineralogy on the sorption of beryllium over time. *Environ. Chem.* http://dx.doi.org/10.1071/EN15107.

Bossew P. and Kirchner G. (2004) Modelling the vertical distribution of radionuclides in soil. Part 1: the convection-dispersion equation revisited. *J. Environ. Radioact.* **73**, 127–150.

Bunzl K., Kracke W. and Schimmack W. (1992) Vertical migration of plutonium-239,-240, americium-241 and caesium-137 fallout in a forest soil under spruce. *Analyst* **117**, 469–474.

Chambers F. M., Mauquoy D., Brain S. A., Blaauw M. and Daniell J. R. G. (2007) Globally synchronous climate change 2800 years ago: Proxy data from peat in South America. *Earth Planet. Sci. Lett.* **253**, 439–444.

Conroy J. L., Overpeck J. T., Cole J. E., Shanahan T. M. and Steinitz-Kannan M. (2008) Holocene changes in eastern tropical Pacific climate inferred from a Galapagos lake sediment record. *Quat. Sci. Rev.* **27**, 1166–1180.

Cutshall N. H., Larsen I. L. and Olsen C. R. (1983) Direct analysis of ^{210}Pb in sediment samples: self-absorption corrections. *Nucl. Instrum. Methods* **206**, 309–312.

Davis R. B., Hess C. T., Norton S. A., Hanson D. W., Hoagland K. D. and Anderson D. S. (1984) ^{137}Cs and ^{210}Pb dating of sediments from soft-water lakes in New England (USA) and Scandinavia, a failure of ^{137}Cs dating. *Chem. Geol.* **44**, 151–185.

Davidson E. A. and Trumbore S. E. (1995) Gas diffusivity and production of CO_2 in deep soils of the eastern Amazon. *Tellus B* **4**, 550–565.

Demers J. D., Blum J. D. and Zak D. R. (2013) Mercury isotopes in a forested ecosystem: implications for air-surface exchange dynamics and the global mercury cycle. *Global Biogeochem. Cycles* **27**, 222–238.

Demirkanli D. I., Molz F. J., Kaplan D. I. and Fjeld R. A. (2009) Soil-root interactions controlling upward plutonium transport in variably saturated soils. *Vadose Zone J.* **8**, 574–585.

Dixon R. K. R., Brown S., Houghton R. A., Solomon A. M., Trexler M. C. and Wisniewski J. (1994) Carbon pools and flux of global forest ecosystems. *Science* **263**, 185–190.

Dorr H. and Munnich K. O. (1989) Downward movement of soil organic matter and its influence on trace element transport. *Radiocarbon* **31**, 655–663.

Dorr H. and Munnich K. O. (1991) Lead and cesium transport in European forest soils. *Water Air Soil Pollut.* **57–58**, 809–818.

Dowdall M., Selnaes G., Gwynn J. P. and Davids C. (2004) Simultaneous determination of ^{226}Ra and ^{238}U in soil and environmental materials by gamma-spectrometry in the absence of radium progeny equilibrium. *J. Radioanal. Nucl. Chem.* **261**, 513–521.

Du P. and Walling D. E. (2012) Using ^{210}Pb measurements to estimate sedimentation rates on river floodplains. *J. Environ. Radioact.* **103**, 59–75.

Dupré de Boulois H., Joner E. J., Leyval C., Jakobsen I., Chen B. D., Roos P., Thiry Y., Rufyikiri G., Delvaux B. and Declerck S. (2008) Role and influence of mycorrhizal fungi on radiocesium accumulation by plants. *J. Environ. Radioact.* **99**, 785–800.

Erel Y., Patterson C. C., Scott M. J. and Morgan J. J. (1990) Transport of industrial lead in snow through soil to stream water and groundwater. *Chem. Geol.* **85**, 383–392.

Eusterhues K., Rumpel C., Kleber M. and Kögel-Knaber I. (2003) Stabilization of soil organic matter by interactions with minerals as revealed by mineral dissolution and oxidative degradation. *Org. Geochem.* **34**, 1591–1600.

EPA (2005) Final combined preliminary assessment/site inspection report for chlor-alkali facility (former), Berlin, New Hampshire. US Environmental Protection Agency, Region 1 Office of Site Remediation and Restoration, Boston MA.

Feely H. W., Larsen R. J. and Sanderson C. G. (1989) Factors that cause seasonal variations in Beryllium-7 concentrations in surface air. *J. Environ. Radioact.* **9**, 223–249.

Ferro-Vázqeuz C., Nóvoa-Muñoz J. C., Costa-Casias M., Klaminder J. and Martínez-Cortizas A. (2014) Metal and organic matter immobilization in temperate podzols: a high-resolution study. *Geoderma* **217–218**, 225–234.

Friedland A. J., Johnson A. H., Siccama T. G. and Mader D. L. (1984) Trace metal profiles in the forest floor of New England. *Soil Sci. Soc. Am. J.* **48**, 422–425.

Gabrieli J., Cozzi G., Vallelonga P., Schwikowski M., Sigl M., Eickenberg J., Wacker L., Boutron C., Gäggeler H., Cescon P. and Barbante C. (2011) Contamination of alpine snow and ice at Colle Gnifetti, Swiss/Italian Alps, from nuclear weapons tests. *Atmos. Environ.* **45**, 587–593.

Graustein W. C. and Turekian K. K. (1989) The effects of forests and topography on the deposition of sub-micrometer aerosols measured by lead-210 and cesium-137 in soils. *Agric. For. Meteorol.* **47**, 199–220.

Graustein W. C. and Turekian K. K. (1990) Radon fluxes from soils to the atmosphere measured by ^{210}Pb–^{226}Ra disequilibrium in soils. *Geophys. Res. Lett.* **17**, 841–844.

Greeman D. J. and Rose A. W. (1996) Factors controlling the emanation of radon and thoron in soils of the eastern U.S.A.. *Chem. Geol.* **129**, 1–14.

Greeman D. J., Rose A. W., Washington J. W., Dobos R. R. and Ciolkosz E. J. (1999) Geochemistry of radium in soils of the Eastern United States. *Appl. Geochem.* **14**, 365–385.

Grondin A., Lucotte M., Fortin B. and Mucci A. (1995) Mercury and lead profiles and burdens in soils of Quebec (Canada) before and after flooding. *Can. J. Fish. Aquat. Sci.* **52**, 2493–2506.

Hansson S. V., Kaste J. M., Chen K. and Bindler R. (2014) Beryllium-7 as a natural tracer for short-term downwash in peat. *Biogeochemistry* **119**, 329–339.

Hardy E. P., Krey P. W. and Volchok H. L. (1973) Global inventory and distribution of fallout plutonium. *Nature* **241**, 444–445.

He Q. and Walling D. E. (1997) The distribution of fallout ^{137}Cs and ^{210}Pb in undisturbed and cultivated soils. *Appl. Radiat. Isot.* **48**, 677–690.

Hirose K., Igarashi Y. and Aoyama M. (2008) Analysis of the 50-year records of the atmospheric deposition of long-lived radionuclides in Japan. *Appl. Radiat. Isot.* **66**, 1675–1678.

Huh C.-A. (1999) Dependence of the decay rate of ^{7}Be on chemical forms. *Earth Planet. Sci. Lett.* **171**, 325–328.

Imboden D. M. and Stiller M. (1982) The influence of radon diffusion on the ^{210}Pb distribution in sediments. *J. Geophys. Res.* **87**, 557–565.

Jiskra M., Wiederhold J. G., Skyllberg U., Kronberg R.-M., Hajdas I. and Kretzschmar R. (2015) Mercury deposition and re-emission pathways in boreal forest soils Investigated with Hg isotope signatures. *Environ. Sci. Technol.* **49**, 7188–7196.

Kaiser K., Guggenberger G., Haumaier L. and Zech W. (2001) Seasonal variations in the chemical composition of dissolved organic matter in organic forest floor layer leachates of old-growth Scots pine (*Pinus sylvestris* L.) and European beech (*Fagus sylvatica* L.) stands in northeastern Bavaria, Germany. *Biogeochemistry*, 103–143.

Kalbitz K. and Kaiser K. (2008) Contribution of dissolved organic matter to carbon storage in forest mineral soils. *J. Plant Nutr. Soil Sci.* **171**, 52–60.

Kaste J. M., Friedland A. J. and Miller E. K. (2005) Potentially mobile lead fractions in montane organic-rich soil horizons. *Water Air Soil Pollut.* **167**, 139–154.

Kaste J. M., Heimsath A. M. and Bostick B. C. (2007) Short-term soil mixing quantified with fallout radionuclides. *Geology* **35**, 243–246.

Kaste J. M., Bostick B. C., Heimsath A. M., Steinnes E. and Friedland A. J. (2011a) Using atmospheric fallout to date organic horizon layers and quantify metal dynamics during decomposition. *Geochim. Cosmochim. Acta* **75**, 1642–1661.

Kaste J. M., Elmore A. J., Vest K. R. and Okin G. S. (2011b) Beryllium-7 in soils and vegetation along an arid precipitation gradient in Owens Valley, California. *Geophys. Res. Lett.* **38**, L09401.

Kato H., Onda Y. and Gomi T. (2012) Interception of the Fukushima reactor accident-derived ^{137}Cs, ^{134}Cs and ^{131}I by coniferous forest canopies. *Geophys. Res. Lett.* **39**, 1–6.

Kerndorff H. and Schnitzer M. (1980) Sorption of metals on humic acid. *Geochim. Cosmochim. Acta* **44**, 1701–1708.

Kersting A. B., Efurd D. W., Finnegan D. L., Rokop D. J., Smith D. K. and Thompson J. L. (1999) Migration of plutonium in groundwater at the Nevada Test Site. *Nature* **397**, 56–59.

Klaminder J. and Yoo K. (2008) Contaminants as tracers for studying dynamics of soil formation: mining an ocean of opportunities. *Adv. Agron.* **100**, 15–57.

Klaminder J., Bindler R., Emteryd O., Appleby P. and Grip H. (2006) Estimating the mean residence time of lead in the organic horizon of boreal forest soils using 210-lead, stable lead and a soil chronosequence. *Biogeochemistry* **78**, 31–49.

Klaminder J., Bindler R., Rydberg J. and Renberg I. (2008) Is there a chronological record of atmospheric mercury and lead deposition preserved in the mor layer (O-horizon) of boreal forest soils? *Geochim. Cosmochim. Acta* **72**, 703–712.

Koide M., Goldberg E. D., Herron M. M. and Langway C. C. (1977) Transuranic depositional history in South Greenland firn layers. *Nature* **269**, 137–139.

Krishnaswamy S., Lal D., Martin J. M. and Meybeck M. (1971) Geochronology of lake sediments. *Earth Planet. Sci. Lett.* **11**, 407–414.

Landis J. D., Hamm N. T., Renshaw C. E., Dade W. B., Magilligan F. J. and Gartner J. D. (2012a) Surficial redistribution of fallout ^{131}iodine in a small temperate catchment. *Proc. Natl. Acad. Sci.* **109**.

Landis J. D., Renshaw C. E. and Kaste J. M. (2012b) Measurement of ^{7}Be in soils and sediments by gamma spectroscopy. *Chem. Geol.* **291**, 175–185.

Landis J. D., Renshaw C. E. and Kaste J. M. (2014) Quantitative retention of atmospherically deposited elements by native vegetation is traced by the fallout radionuclides ^{7}Be and ^{210}Pb. *Environ. Sci. Technol.* **48**, 12022–12030.

Likuku A. S. (2009) Atmospheric transfer and deposition mechanisms of ^{210}Pb aerosols onto forest soils. *Water Air Soil Pollut.* **9**, 179–184.

Livingston H. D., Schneider D. L. and Bowen V. T. (1975) ^{241}Pu in the marine environment by a radiochemical procedure. *Earth Planet. Sci. Lett.* **25**, 361–367.

Ma L., Konter J., Herndon E., Jin L., Steinhofel G., Sanchez D. and Brantley S. (2014) Quantifying an early signature of the industrial revolution from lead concentrations and isotopes in soils of Pennsylvania, USA. *Anthropocene* **7**, 16–29.

Mabit L., Benmansour M., Abril J. M., Walling D. E., Meusburger K., Iurian A. R., Bernard C., Tarján S., Owens P. N., Blake W. H. and Alewell C. (2014) Fallout ^{210}Pb as a soil and sediment tracer in catchment sediment budget investigations: a review. *Earth Sci. Rev.* **138**, 335–351.

Mackay A., Battarbee R., Birks J. and Oldfield F. (2014) *Global Change in the Holocene*. Routledge Press, New York.

Mason R. P., Fitzgerald W. F. and Morel F. M. M. (1994) The biogeochemical cycling of elemental mercury: anthropogenic influences. *Geochim. Cosmochim. Acta* **58**, 3191–3198.

Matisoff G. (2014) ^{210}Pb as a tracer of soil erosion, sediment source area identification and particle transport in the terrestrial environment. *J. Environ. Radioact.* **138**, 343–354.

Matisoff G., Wilson C. G. and Whiting P. J. (2005) The ^{7}Be/^{210}Pb$_{xs}$ ratio as an indicator of suspended sediment age or fraction new sediment in suspension. *Earth Surf. Process. Landforms* **30**, 1191–1201.

Matisoff G., Ketterer M. E., Rosén K., Mietelski J. W., Vitko L. F., Persson H. and Lokas E. (2011) Downard migration of Chernobyl-derived radionuclides in soils in Poland and Sweden. *Appl. Geochem.* **26**, 105–115.

Matsuda N., Mikami S., Shimoura S., Takahashi J., Nakano M., Shimada K., Uno K., Hagiwara S. and Saito K. (2015) Depth profiles of radioactive cesium in soil using a scraper plate over a wide area surrounding the Fukushima Dai-ichi Nuclear Power Plant, Japan. *J. Environ. Radioact.* **139**, 427–434.

Miller E. K. and Friedland A. J. (1994) Lead migration in forest soils: response to changing atmospheric inputs. *Environ. Sci. Technol.* **28**, 662–669.

Murozumi M., Chow T. S. and Patterson C. (1969) Chemical concentrations of pollutant lead aerosols, terrestrial dusts and sea salts in Greenland and Antarctic snow strata. *Geochim. Cosmochim. Acta* **33**, 1247–1294.

Nriagu J. O. (1988) A silent epidemic of environmental metal poisoning? *Environ. Pollut.* **50**, 139–161.

Nriagu J. O. and Pacyna J. M. (1988) Quantitative assessment of worldwide contamination of air, water and soils by trace metals. *Nature* **336**, 403–405.

Obrist D., Johnson D. W., Lindberg S. E., Luo Y., Hararuk O., Bracho R., Battles J. J., Dail D. B., Edmonds R. L., Monson R. K., Ollinger S. V., Pallardy S. G., Pregitzer K. S. and Todd D. E. (2011) Mercury distribution across 14 U.S. Forests. Part I: spatial patterns of concentrations in biomass, litter, and soils. *Environ. Sci. Technol.* **45**, 3974–3981.

Olivier S., Bajo S., Fifield L. K., Gäggeler H. W., Papina T., Santschi P. H., Schotterer U., Schwikowski M. and Wacker L. (2004) Plutonium from global fallout recorded in an ice core from the Belukha Glacier, Siberian Altai. *Environ. Sci. Technol.* **38**, 6507–6512.

Olsen C. R., Larsen I. L., Lowry P. D., Cutshall N. H., Todd J. F., Wong G. T. F. and Casey W. H. (1985) Atmospheric fluxes and marsh-soil inventories of ^{7}Be and ^{210}Pb. *J. Geophys. Res.* **90** (D6), 10487–10495.

Penrose W. R., Polzer W. L., Essington E. H., Nelson D. M. and Orlandini K. A. (1990) Mobility of plutonium and americium through a shallow aquifer in a semiarid region. *Environ. Sci. Technol.* **24**, 228–234.

Pietrzak-Flis Z., Radwan I., Rosiak L. and Wirth E. (1996) Migration of ^{137}Cs in soils and its transfer to mushrooms and vascular plants in mixed forest. *Sci. Total Environ.* **186**, 243–250.

Pokrovsky O. S., Dupré B. and Schott J. (2005) Fe-Al-organic colloids control of trace elements in peat soil solutions: results of ultrafiltration and dialysis. *Aquat. Geochem.* **11**, 241–278.

Preiss N., Melieres M.-A. and Pourchet M. (1996) A compilation of data on lead-210 concentration in surface air and fluxes at the air-surface and water-sediment interfaces. *J. Geophys. Res.* **101**, 28847–28862.

Prestbo E. M. and Gay D. A. (2009) Wet deposition of mercury in the U.S. and Canada, 1996–2005: results and analysis of the NADP mercury deposition network (MDN). *Atmos. Environ.* **43**, 4223–4233.

Robbins, J. A. (1978) Geochemical and geophysical applications of radioactive lead isotopes. In *Biogeochemistry of Lead* (ed. J. P. Nriago). North Holland, Amsterdam, pp 285–393.

Rosén K., Öborn I. and Lönsjö H. (1999) Migration of radiocaesium in Swedish soil profiles after the Chernobyl accident, 1987–1995. *J. Environ. Radioact.* **46**, 45–66.

Sanchez A. L., Wright S. M., Smolders E., Naylor C., Stevens P. A., Kennedy V. H., Dodd B. A., Singleton D. L. and Barnett C. L. (1999) High plant uptake of radiocesium from organic soils due to Cs mobility and low soil K content. *Environ. Sci. Technol.* **33**, 2752–2757.

Sanchez-Cabeza J. A., Ani-Ragolta I. and Masqué P. (2000) Some considerations of the ^{210}Pb constant rate of supply (CRS) dating model. *Limnol. Oceanogr.* **45**, 990–995.

Santschi P. H., Allison M. A., Asbill S., Perlet A. B., Cappellino S., Dobbs C. and Mcshea L. (1999) Sediment transport and Hg recovery in Lavaca Bay, as evaluated from radionuclide and Hg distributions. *Environ. Sci. Technol.* **33**, 378–391.

Santschi P. H., Roberts K. A. and Guo L. D. (2002) Organic nature of colloidal actinides transported in surface water environments. *Environ. Sci. Technol.* **36**, 3711–3719.

Schimel D. S. (1995) Terrestrial ecosystems and the carbon cycle. *Global Change Biol.* **1**, 77–91.

Schmidt M. W. I., Torn M. S., Abiven S., Dittmar T., Guggenberger G., Janssens I. A., Kleber M., Kögel-Knabner I., Lehmann J., Manning D. A. C., Nannipieri P., Rasse D. P., Weiner S. and Trumbore S. E. (2011) Persistence of soil organic matter as an ecosystem property. *Nature* **478**, 49–56.

Shakhashiro A. and Mabit L. (2009) Results of an IAEA intercomparison exercise to assess ^{137}Cs and total ^{210}Pb analytical performance in soil. *Appl. Radiat. Isot.* **67**, 139–146.

Simon S. L., Bouville A. and Beck H. L. (2004) The geographic distribution of radionuclide deposition across the continental US from atmospheric nuclear testing. *J. Environ. Radioact.* **74**, 91–105.

Stankwitz C., Kaste J. M. and Friedland A. J. (2012) Threshold increases in soil lead and mercury from tropospheric deposition across an elevational gradient. *Environ. Sci. Technol.* **46**, 8061–8068.

Steiner M., Linkov I. and Yoshida S. (2002) The role of fungi in the transfer and cycling of radionuclides in forest ecosystems. *J. Environ. Radioact.* **58**, 217–241.

Steinnes A. J. and Friedland E. (2005) Lead migration in Podzolic soils from Scandinavia and the United States of America. *Can. J. Soil Sci.* **85**, 291–294.

Steinnes E. and Friedland A. J. (2006) Metal contamination of natural soils from long-range atmospheric transport: existing and missing knowledge. *Environ. Rev.* **14**, 169–186.

Takahashi Y., Minai Y., Ambe S., Makide Y. and Ambe F. (1999) Comparison of adsorption behavior of multiple inorganic ions on kaolinite and silica in the presence of humic acid using the multitracer technique. *Geochim. Cosmochim. Acta* **63**, 815–836.

Taylor A., Blake W. H., Smith H. G., Mabit L. and Keith-Roach M. J. (2013) Assumptions and challenges in the use of fallout beryllium-7 as a soil and sediment tracer in river basins. *Earth Sci. Rev.* **126**, 85–95.

Todorov B. and Djingova R. (2015) Fractionation and soil-plant transfer of ^{241}Am in different soil types. *Pedosphere* **25**, 212–219.

Tyler G. (2004) Ionic charge, radius, and potential control root/soil concentration ratios of fifty cationic elements in the organic horizon of beech (*Fagus sylvatica*) forest podzol. *Sci. Total Environ.* **329**, 231–239.

Thompson A., Chadwick O. A., Boman S. and Chorover J. (2006) Colloid mobilization during soil iron redox oscillations. *Environ. Sci. Technol.* **40**, 5743–5749.

UNSCEAR (2000) United Nations Scientific Committee on the Effects of Atomic Radiation, Volume 1: Sources and Effects of Ionizing Radiation, Annex C: Exposures to the Public from Man-Made Sources of Radiation, Vienna, Austria.

Wallbrink P. J. and Murray A. S. (1996) Distribution and variability of ^{7}Be in soils under different surface cover conditions and its potential for describing soil redistribution processes. *Water Resour. Res.* **32**, 467–476.

Walling D. E. (2013) Beryllium-7: The Cinderella of fallout radionuclide sediment tracers? *Hydrol. Process.* **27**, 830–844.

Walling D. E., Schuller P., Zhang Y. and Iroumé A. (2009) Extending the timescale for using beryllium-7 measurements to document soil redistribution by erosion. *Water Resour. Res.* **45**, 1–13.

Wang E. X. and Benoit G. (1997) Fate and transport of contaminant lead in spodosols: a simple box model analysis. *Water Air Soil Pollut.* **95**, 381–397.

Wang C., Hou S., Pang H., Liu Y., Gäggeler H. W., Tobler L., Szidat S. and Vogel E. (2014) ^{210}Pb dating of the Miaoergou ice core from the eastern Tien Shan, Chia. *Ann. Glaciol.* **55**, 105–110.

Wang Z. T., Zheng J., Tagami J. and Uchida S. (2015) Newly derived transfer factors for Th, Am, Pu, and Cl since publication of IAEA TRS No. 472: a review. *J. Radionanal. Nucl. Chem.* **306**, 11–20.

Warneke T., Croudace I. W., Warwick P. E. and Taylor R. N. (2002) A new ground-level fallout record of uranium and plutonium isotopes for northern temperate latitudes. *Earth Planet. Sci. Lett.* **203**, 1047–1057.

Yasunari T. J., Stohl A., Hayano R. S., Burkhart J. F., Eckhardt S. and Yasunari T. (2011) Cesium-137 deposition and contamination of Japanese soils due to the Fukushima nuclear accident. *Proc. Natl. Acad. Sci.* **108**, 19530–19534.

You C., Lee T. and Li Y. (1989) The partition of Be between soil and water. *Chem. Geol.* **77**, 105–118.

Zabowski D. and Ugolini F. C. (1990) Lysimeter and centrifuge soil solutions: seasonal differences between methods. *Soil Sci. Soc. Am. J.* **54**, 1130–1135.

Zhang W., Ungar K., Chen J., St-Amant N. and Tracy B. L. (2009) An accurate method for the determination of ^{226}Ra activity concentrations in soil. *J. Radioanal. Nucl. Chem.* **280**, 561–567.

Associate editor: Anthony Dosseto